

# Highly Efficient, Dendrite-Free Zinc Electrodeposition in Mild Aqueous Zinc-Ion Batteries through Indium-Based Substrates

Michele Tribbia,<sup>[a]</sup> Jens Glenneberg,<sup>[b]</sup> Giorgia Zampardi,<sup>\*[a]</sup> and Fabio La Mantia<sup>\*[a, b]</sup>

Quasi-neutral aqueous zinc-ion (Zn-ion) batteries are nowadays among the most promising energy storage devices for smart-grid applications. However, their practical use remains hindered by the low Zn electrodeposition efficiency at the negative electrode, which is especially reduced due to the parasitic evolution of gaseous hydrogen. Indium is a non-toxic metal showing poor hydrogen evolution kinetics, but it is also very expensive. Therefore, an optimized mixture of bismuth and

indium particles has been used as the substrate for the Zn electrodeposition and dissolution reaction to increase its reversibility and its efficiency in a quasi-neutral ZnSO<sub>4</sub> solution. This strategy not only allowed to prolong the cycle life of a full Zn-ion cell of 10 times at 0.5 C due to the suppression of the hydrogen evolution reaction, as proved by the *operando* DEMS analysis, but also led to very homogeneous zinc deposits over prolonged cycling at realistic charge and current densities.

## Introduction

The massive inclusion of renewable energy sources in the energy market is mainly limited by their volatile nature. To overcome this problem, stationary battery systems are employed to store the over-generated electric power and to release it on demand when needed.<sup>[1,2]</sup> Aqueous metal-ion batteries are among the most appropriate systems for stationary applications not only thanks to their environmental friendliness, but also since the high ionic conductivity of the aqueous electrolyte allows high power densities of the final cell.<sup>[3,4]</sup> Further advantages of these systems are related to their low production and material costs and intrinsic high safety.<sup>[1,5-8]</sup>

Among the different aqueous metal-ion batteries, mild aqueous zinc-ion batteries (ZIBs) have attracted great attention because of the high theoretical specific capacity (5855 mAh cm<sup>-3</sup>) and low standard reduction potential ( $-0.76$  V vs. SHE) of the metallic zinc,<sup>[6,8-10]</sup> together with the low estimated cost of the overall cell ( $< 65$  \$ kWh<sup>-1</sup>).<sup>[7]</sup> However, despite the first rechargeable mild-aqueous ZIB was developed by Yamamoto in 1986,<sup>[11]</sup> this technology has not reached the

market yet, mostly because of the low efficiency of the Zn electrodeposition/dissolution reaction occurring at the cell's negative electrode (often referred to as "anode"). In particular, the Zn electrodeposition reaction not only is often characterized by the formation of sharp dendrites, but also by a concomitant and especially unwanted evolution of gaseous hydrogen from the water-based electrolyte. The former phenomenon leads to an internal short circuit of the cell, while the latter to pressure build-ups and to a decreased Coulombic efficiency that remains too low to provide a prolonged battery lifespan. Moreover, the hydrogen evolution reaction alters the local pH in the proximity of the zinc-based electrode's surface, thus inducing an unwanted formation of inactive zinc oxides/hydroxides-based species and, in the commonly used sulphate-based electrolytes, of zinc hydroxy sulphates.<sup>[7,12-16]</sup> Therefore, the effective capacity of the zinc-based electrode is reduced, and Zn<sup>2+</sup> ions are irreversibly removed from the solution and thus not available for the main reactions of the Zn-ion battery.

Several methods have been suggested to improve the Zn electrodeposition/dissolution efficiency, such as the use of porous substrates,<sup>[17-21]</sup> inert scaffolds or additives in the solid electrode,<sup>[22-25]</sup> supporting electrolytes,<sup>[26]</sup> Zn-host materials,<sup>[27,28]</sup> organic additives in the electrolyte,<sup>[29,30]</sup> ionic liquids,<sup>[31]</sup> concentrated electrolytes,<sup>[32]</sup> artificial electrode-electrolyte interphases,<sup>[33]</sup> and membranes.<sup>[34]</sup> Despite high performance and good reversibility of the zinc electrodeposition reaction have been sometimes claimed,<sup>[21,26,32]</sup> the use of expensive solid additives and concentrated electrolytes does not match the requirements of easy manufacturing, low-cost processes and environmental sustainability that are strictly dictated by the stationary energy sector.<sup>[28,35]</sup> Moreover, the capacity limit and the current applied during the analysis of the zinc electrodeposition reaction are not always carefully considered,<sup>[6,14,35,36]</sup> even if the zinc electrodeposition reaction strongly depends on them.<sup>[35]</sup> In particular, the role of the current density applied during the Zn electrodeposition/dissolution cycles has a

[a] M. Tribbia, Dr. G. Zampardi, Prof. F. La Mantia  
Energiespeicher- und Energiewandlersysteme  
Universität Bremen  
Bibliothekstraße 1, 28359 Bremen, Germany  
E-mail: zampardi@uni-bremen.de  
lamantia@uni-bremen.de

[b] Dr. J. Glenneberg, Prof. F. La Mantia  
Fraunhofer Institute for Manufacturing Technology and Advanced Materials  
– IFAM  
Wiener Str. 12, 28359, Bremen, Germany

Supporting information for this article is available on the WWW under  
<https://doi.org/10.1002/batt.202100381>

© 2022 The Authors. *Batteries & Supercaps* published by Wiley-VCH GmbH. This is an open access article under the terms of the Creative Commons Attribution Non-Commercial NoDerivs License, which permits use and distribution in any medium, provided the original work is properly cited, the use is non-commercial and no modifications or adaptations are made.

tremendous effect on the homogeneity of the Zn deposits. Frequently, low current densities of ca.  $1 \text{ mA cm}^{-2}$  are applied during the deposition/dissolution cycles to avoid the formation of dendrites. Another strategy often invoked in the literature is applying higher current densities ( $> 5 \text{ mA cm}^{-2}$ ) for a short time or low capacity limits, thus depositing/dissolving only a little amount of metallic zinc.<sup>[35]</sup> Unfortunately, both strategies despite maximizing the performance of the zinc electrode provide misleading results as they do not resemble the real working conditions envisaged for stationary energy storage applications. In fact, in this case, the Zn-ion cell should have a capacity ratio of the negative electrode and the positive electrode close to the unit, and it should be able to absorb high load peaks at the same time (peak shaving).<sup>[37]</sup> Both of these realistic operating conditions may lead to a dead battery earlier than expected according to the performances reported in the literature.<sup>[35,37]</sup>

Moreover, the occurrence of the parasitic hydrogen evolution reaction is often ignored when discussing the Zn electrodeposition efficiency. It has been demonstrated, that the unwanted, although thermodynamically favored, hydrogen evolution takes place during the Zn electrodeposition step and leads to local pH changes in correspondence of the Zn-based electrode, promoting the formation of inactive and/or poorly conductive zinc passivation species.<sup>[13,38]</sup> This causes not only a strong decrease of the Coulombic efficiency of the Zn electrode, and therefore of the overall Zn-ion cell, but also the irreversible loss of  $\text{Zn}^{2+}$  ions from the electrolytic solution. Due to its detrimental effects on the overall Zn-ion cell, especially when electrodes having a porous structure with a high surface area are employed, the suppression of the hydrogen evolution reaction is a challenge that must be specifically tackled. To suppress the parasitic hydrogen evolution reaction and to consequently promote a homogeneous and highly efficient deposition of metallic zinc during the battery operation, electrodes constituted by metallic indium particles have been employed as a substrate for the Zn electrodeposition/dissolution. The advantage of choosing indium as a possible substrate for the Zn electrodeposition is related to its low exchange current density for the hydrogen evolution reaction (reported in previous work<sup>[39]</sup>), which is translated in very poor reaction kinetics.<sup>[39]</sup> However, as envisaging the use of bulk indium electrodes would severely increase the final cost of an aqueous Zn-ion cell, a different substrate based on cost-effective metallic bismuth particles containing a reduced amount of metallic indium has been employed as well. Galvanostatic cycling has been performed in order to visualize the cycling behavior of the different electrodes and to estimate their Zn

electrodeposition efficiency. All the substrates used for the Zn electrodeposition have been tested within a mild-acidic aqueous electrolyte (500 mM  $\text{ZnSO}_4$ ,  $\text{pH} \approx 5$ ), and their performance has been compared to the one of a standard zinc powder electrode operated in the same experimental conditions. Moreover, crystallographic and morphological analysis has been performed on the pristine and the cycled substrates to visualize the evolution of the morphology of the deposited zinc, together with the formation of any unwanted Zn-based species. The bismuth-indium electrodes have then been used within a full Zn-ion pouch-cell, whose configuration is closer to real-life applications, to estimate the practical feasibility of this concept. Moreover, the amount of gaseous hydrogen evolved during the operation of the full cell Zn-ion cell has been quantified through *operando* differential electrochemical mass spectrometry (DEMS). Finally, an extensive comparison with the state-of-the art substrates for the Zn electrodeposition/dissolution reaction for aqueous Zn-ion batteries has been carried out, further confirming the excellent performance of the Bi–In-powder electrode employed within this work.

## Results and Discussion

Initially, a Zn-powder electrode mainly constituted of metallic zinc particles, whose exact composition is shown in Table 1, has been galvanostatically cycled in 500 mM  $\text{ZnSO}_4$  with an applied current of  $4.1 \text{ mA cm}^{-2}$ , corresponding to a depth of discharge of 50% (Figure 1a). After the initial cycles, a cathodic potential spike increasing with the number of cycles can be observed at the very beginning of the Zn deposition step. Such abrupt potential drop is caused by a partial reduction of Zn oxide/hydroxide-based species to metallic zinc.<sup>[25]</sup> These unwanted species are formed and stabilized by the local increase of pH in correspondence of the surface of the Zn-powder electrode due to the occurrence of the parasitic hydrogen evolution reaction,<sup>[13,38]</sup> which consequently leads to a decrease of the Zn-electrodeposition efficiency. The Zn-electrodeposition efficiency is the ratio between the oxidation (Zn dissolution step) and the reduction (Zn deposition step) charge flow. As shown in Figure 1(b), the Zn electrodeposition efficiency of the Zn-powder electrode remained at ca. 100% only during the initial 10 cycles, when an excess of metallic zinc is present on the electrode. Afterwards, it decreased abruptly to a value of ca. 90%, which has been attributed to an irreversible formation of zinc oxide/hydroxide-based species.<sup>[13,25]</sup>

In order to hinder the hydrogen evolution reaction during the Zn plating step, an electrode mainly constituted of indium

**Table 1.** Weight percentage of the materials constituting all powder composite electrodes that have been investigated in the frame of this work.

Electrode	Zinc	Bismuth	Indium	C65	PVDF
Zn-powder	90	—	—	5	5
C-powder	—	—	—	50	50
Bi-powder	—	90	—	5	5
In-powder	—	—	90	5	5
Bi-In	—	80	10	5	5

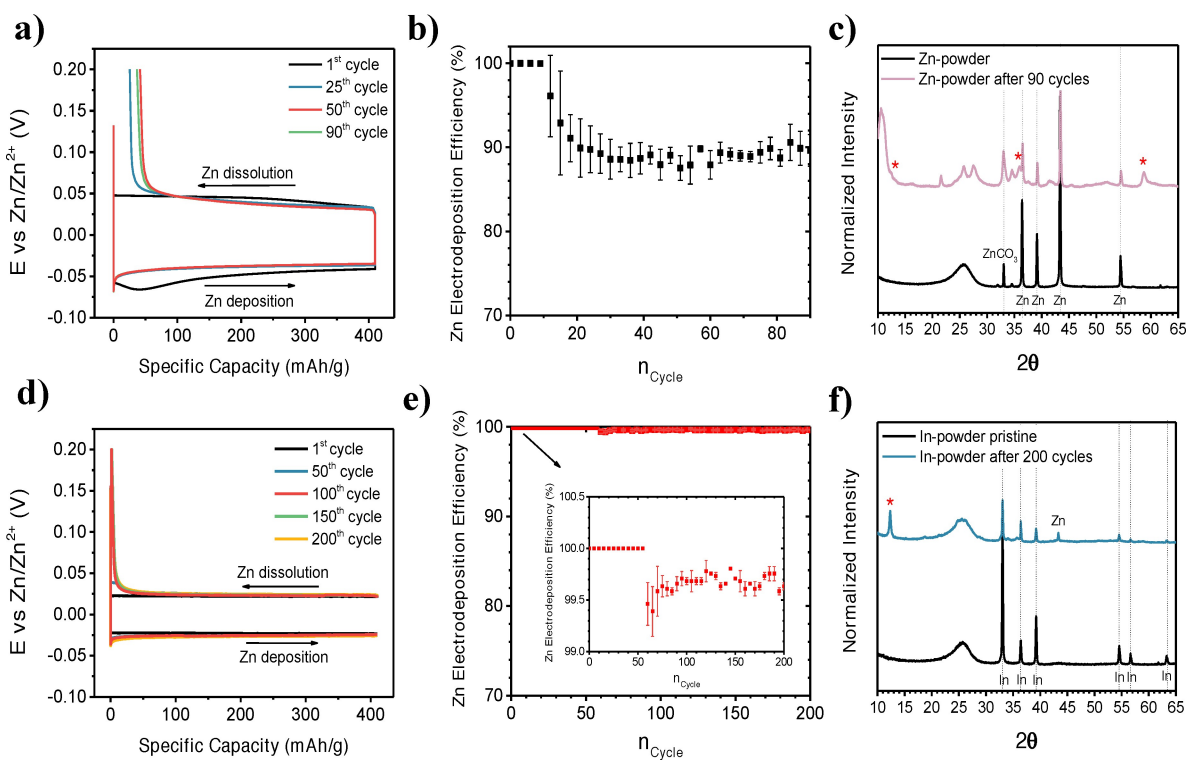


**Figure 1.** a) Galvanostatic cycles, b) average zinc electrodeposition efficiency and c) XRD pattern of a Zn-powder electrode cycled in 500 mM ZnSO<sub>4</sub>. d) Galvanostatic cycles, e) average zinc electrodeposition efficiency and f) XRD pattern of a In-powder electrode cycled in 500 mM ZnSO<sub>4</sub>. The stripping/plating current corresponded in both cases to a depth of discharge of 50 %. The mean values of the Coulombic efficiency together with their relative standard deviations have been calculated from the results of three different experiments. The reflections in the XRD pattern corresponding to zinc hydroxy sulphate Zn<sub>4</sub>(OH)<sub>6</sub>SO<sub>4</sub>·nH<sub>2</sub>O have been marked with (\*).

particles, whose exact composition is shown in Table 1, has been chosen as the substrate for the Zn electrodeposition/dissolution reaction. It is commonly known that the evolution of hydrogen is kinetically unfavored on metallic indium, due to the low exchange current density characterizing this metal, whose value is reported in previous reference.<sup>[39]</sup> The galvanostatic profile of the Zn electrodeposition/dissolution reaction onto In-powder electrodes is shown in Figure 1(d). During the galvanostatic cycling, a current of 2.05 mA cm<sup>-2</sup>, corresponding to a depth of discharge of 50 %, was applied to the In-powder electrode for the Zn dissolution/deposition cycles. Interestingly, no cathodic spike could be observed in the galvanostatic cycles at the very beginning of the reduction step (i.e., Zn deposition), indicating that the zinc oxide/hydroxides-based species<sup>[13,25]</sup> are not appreciably stable at the surface of the In-powder substrate, compared to the Zn-powder one.

As shown in Figure 1(e), the Coulombic efficiency of the Zn electrodeposition/dissolution reaction onto In-powder substrates was 100% during the initial 50 cycles and it remained at ca. 99.8% until the end of the experiment (200 cycles). Such striking increase of the Zn electrodeposition efficiency is most likely due to the suppression of the hydrogen evolution reaction thanks to its poor kinetics on metallic indium.<sup>[39]</sup> This therefore prevents the local pH increase in the proximity of the surface of the electrode, thus hindering the formation of passivating Zn oxide/hydroxide-based species that cause an irreversible loss of Zn<sup>2+</sup>.

Crystallographic analysis was performed onto the pristine and cycled In-powder electrode, as shown in Figure 1(f). It is worth noticing that after 200 cycles, the reflections of the indium did not undergo any significant shift, indicating that the metallic indium did not form an alloy with the zinc upon the Zn deposition/dissolution cycles. A peak related to the zinc hydroxy sulphate<sup>[40]</sup> (Zn<sub>4</sub>(OH)<sub>6</sub>SO<sub>4</sub>·nH<sub>2</sub>O) is visible within the diffractogram of the cycled In-powder electrode after 200 cycles. In the case of the cycled Zn-powder electrode (Figure 1c), peaks related to different hydrated phases of zinc hydroxy sulphate<sup>[40]</sup> are visible after 90 cycles.

From a morphological point of view, the deposition of zinc looked very homogeneous on In-powder substrates, as demonstrated by the SEM images shown in Figure 2. Initially, the morphology of a pristine In-powder electrode was characterized by large flat flakes of metallic Indium onto the carbon fibers constituting the current collector (Figure 2a). These large flakes are coalesced indium particles that had been formed during the mixing step of the liquid slurry made with a turbo mixer, because of the characteristic softness of metallic indium. After 200 cycles, the In-powder substrate retained a morphology very similar to its uncycled state, as shown in Figure 2(b) and c). On the contrary, after only 90 cycles the morphology of the whole Zn-powder electrode was characterized by deposits with a hexagonal lamellar shape, which is typical of the layered double hydroxides,<sup>[25,41]</sup> such as the inactive zinc hydroxy sulphate.<sup>[25,41]</sup> This clay-like compound is a common passivation

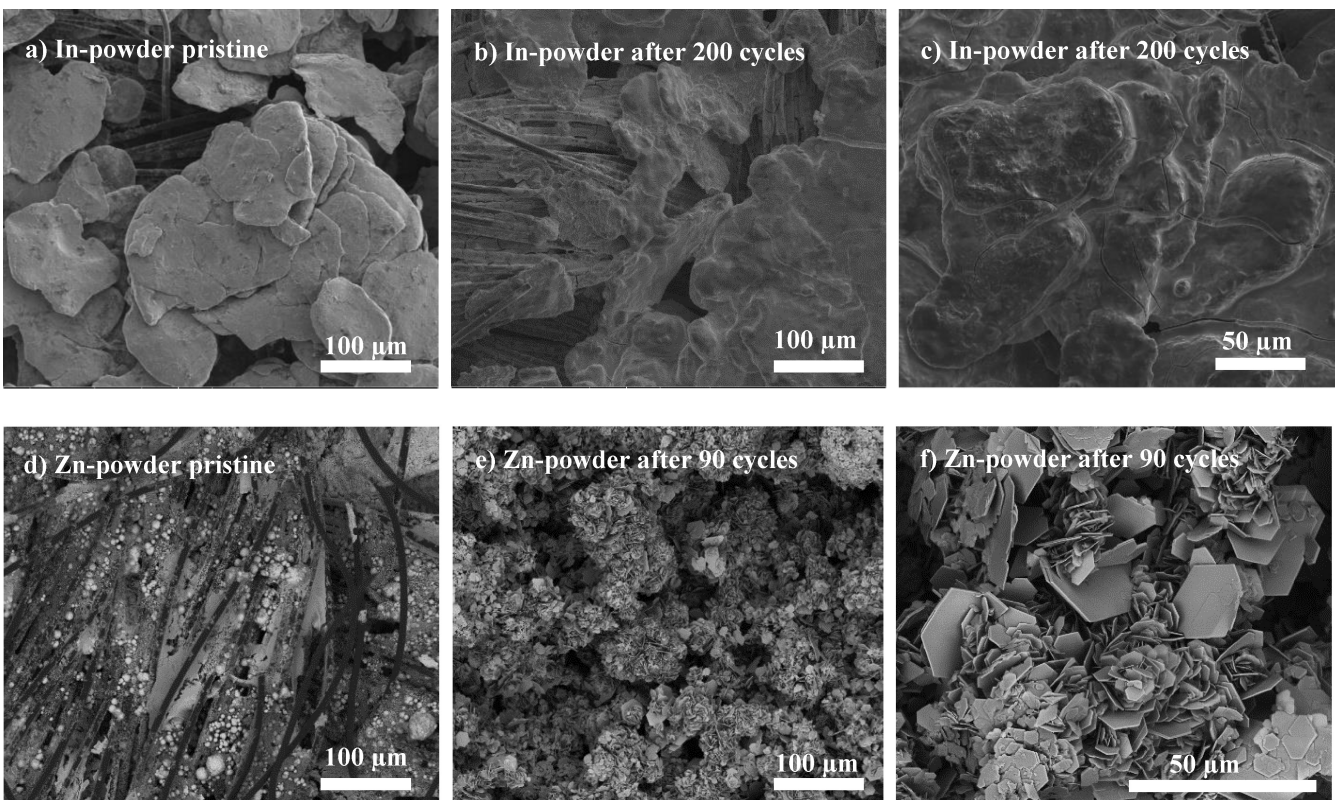


**Figure 2.** SEM images of an In-powder electrode a) before and b, c) after 200 galvanostatic cycles in 500 mM ZnSO<sub>4</sub>. SEM images of a Zn-powder electrode d) before and e, f) after 90 galvanostatic cycles in 500 mM ZnSO<sub>4</sub>. All the SEM images of the cycled electrodes have been acquired after a Zn-stripping step.

product of metallic zinc, whose formation takes place in sulphate-containing electrolytes when the pH of the solution reaches a value of ca. 5.5–6.<sup>[42–44]</sup> The local increase of the pH is the result of the reduction of the hydronium ions to gaseous hydrogen.<sup>[13]</sup> Therefore, the evolution of the initial electrode's morphology to a lamellar one can be considered as an indicator of the extent of the hydrogen evolution reaction and thus it supports the observed much lower Zn electrodeposition efficiency of the Zn-powder electrode compared to the In-powder one.<sup>[25,41]</sup>

Despite the outstanding efficiency reached by the zinc electrodeposition reaction using In-powder electrodes, such substrates although non-toxic are not very appealing for a real-life application, due to the high market price of metallic indium. As reported in previous work,<sup>[45]</sup> the market price of metallic indium was ca. 180 \$ kg<sup>-1</sup> in December 2020, that is ca. 50 times higher than the one of metallic zinc (3.5 \$ kg<sup>-1</sup> in December 2020 as well).<sup>[46]</sup> Therefore, the strategy to be followed is to reduce the amount of metallic indium within the electrode formulation, while keeping at the same time a high zinc electrodeposition efficiency. For this reason, electrodes mainly constituted of metallic bismuth particles containing only 10% in weight of indium particles (the exact composition of the Bi–In-powder electrodes can be found in Table 1) have been prepared and galvanostatically tested, as shown in Figure 3. The choice of the lowest amount of indium particles was based on a preliminary analysis of the zinc electro-

deposition efficiency of three different Bi–In powder electrodes containing 5 wt%, 10 wt% and 15 wt% of metallic indium, respectively (Figure SI\_1 of the Supporting Information, Section 1).

Metallic bismuth has been chosen in order to have a chemically stable substrate that could ensure a uniform electric field on the surface of the electrode during the Zn electrodeposition and dissolution cycles. Moreover, metallic bismuth is non-toxic, environmentally friendly and its low market price of ca. 5.7 \$ kg<sup>-1</sup> is very close to the one of metallic zinc.<sup>[45,46]</sup> In terms of kinetics towards the hydrogen evolution reaction, bismuth exhibits an exchange current density similar to the one of metallic zinc, whose values are reported in previous work.<sup>[39]</sup> In fact, the zinc deposition onto Bi-powder electrodes containing only bismuth particles (whose exact composition is shown in Table 1), is similar to the one observed onto Zn-powder electrodes in terms of efficiency and morphology evolution. An initial amount of 5 mg of metallic zinc was electrodeposited from a 500 mM ZnSO<sub>4</sub> solution onto the Bi-powder substrate prior to the galvanostatic cycling. The Zn electrodeposition efficiency onto Bi-powder substrates remained ca. 90% for the initial 150 Zn deposition/dissolution cycles, afterwards it dropped to ca. 85% until the end of the measurement (200 cycles), as shown in Figure SI\_2 in the Supporting Information, Section 2. Moreover, the XRD pattern of the Bi-powder electrode recorded after 100 cycles showed the peaks related to the zinc hydroxy sulphate (Figure SI\_3,

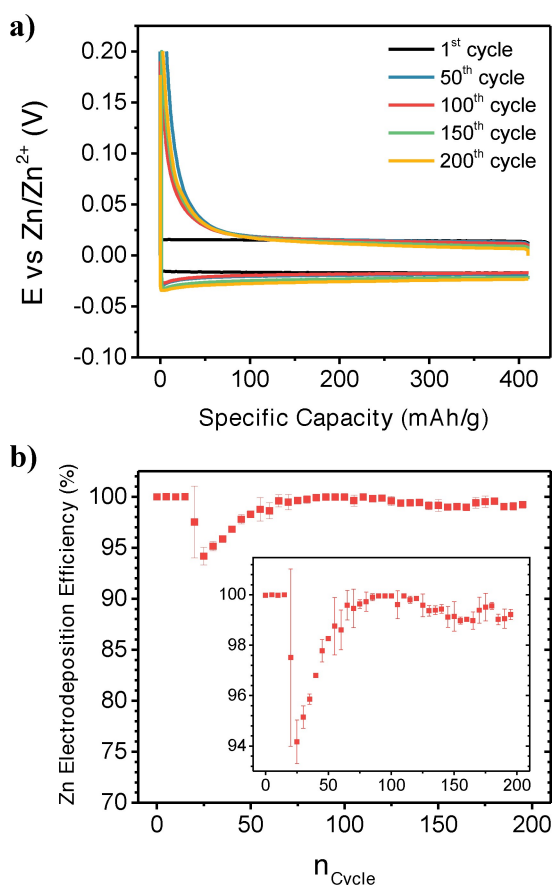


**Figure 3.** a) Galvanostatic cycles and b) average zinc electrodeposition efficiency of a Bi–In-powder electrode in 500 mM ZnSO<sub>4</sub>. The mean values of the Coulombic efficiency together with their relative standard deviations have been calculated from the results of three different experiments.

Section 3 of the Supporting Information). The morphology of the Bi-powder electrode changed dramatically during the Zn deposition/dissolution cycles as well: similar to the Zn-powder electrode, the initial morphology of a Bi-powder electrode was characterized by bismuth round particles onto the carbon fibers constituting the carbon cloth current collector. After only 100 Zn deposition/dissolution cycles, the whole Bi-powder electrode was entirely covered with lamellar-shaped deposits, typical of the layered double hydroxides,<sup>[25,41]</sup> such as the zinc hydroxy sulphate (Figure SI\_4, Supporting Information, Section 4).<sup>[25,41]</sup>

It is worth noticing that, despite the Coulombic efficiency and the morphology evolution of the Bi-powder electrode are similar to the Zn-powder one, bismuth has been chosen as main metallic component of the Bi–In powder substrate for the Zn deposition/dissolution reaction to ensure high mechanical and electrical stability of the electrode. Contrary to the Zn particles, Bi particles do not dissolve during the Zn dissolution/deposition reaction, thus keeping the electrode mechanically stable and maintaining the electrical contact with the current collector during subsequent galvanostatic cycles.

The Zn electrodeposition/dissolution cycles of the Bi–In-electrode are shown in Figure 3(a). Also in this case, an initial amount of 5 mg of metallic zinc was electrodeposited from a

500 mM ZnSO<sub>4</sub> solution onto the Bi–In-powder substrate prior to the galvanostatic cycling, since the Bi–In-powder electrode did not contain any metallic Zn reservoir within its original formulation. During the galvanostatic cycling, a current corresponding to a depth of discharge of 50% was applied to the Bi–In-powder electrode. It is worth noticing that as in the case of the In-powder electrode, no initial cathodic spike could be observed within the galvanostatic cycles of the Bi–In-powder electrodes at the very beginning of the Zn deposition step (Figure 3a). This suggests that also in this case the zinc passivation species are not appreciably stable on the surface of the Bi–In-electrode.<sup>[25]</sup> Thanks to the addition of 10 wt% of metallic indium particles within the electrode formulation, the zinc electrodeposition efficiency remained at 100% during the initial 15 cycles, then it dropped to 94% at the 25<sup>th</sup> cycle, and it subsequently increased to a value around ca. 99.4% until the end of the experiment (200 cycles), as shown in Figure 3(b). Such Coulombic efficiency drop between the 25<sup>th</sup> and the 50<sup>th</sup> cycle could be due to the consumption of the metallic zinc previously deposited onto the Bi–In-based substrate or to the initial precipitation of passivation products onto the surface of the deposited metallic zinc layer. However, the amount of metallic indium present within the substrate's formulation was enough to efficiently hinder the formation of an appreciable amount of Zn passivation products even in presence of a metallic zinc reservoir, since after the 50<sup>th</sup> cycle the Zn electrodeposition efficiency remained stable around ca. 99.4% until the end of the measurement (200 cycles). It is worth noticing that such initial drop of Coulombic efficiency of ca. 5% is visible thanks to the appropriately magnified scale and the appropriate small dimension of the used markers in Figure 3(b). It is difficult to compare this result with the ones already reported in the literature, as unfortunately the Coulombic efficiency is routinely represented not only with a scale ranging from 0% to >120%, but also with the aid of markers having a dimension of ca. 5%. As a result, even in the case that such small fluctuations of the Coulombic efficiency exist, this kind of widely used inappropriate representation makes them impossible to be seen. The crystallographic analysis performed on the pristine and cycled Bi–In-powder electrode is shown in Figure 4(a). The diffractogram of the pristine electrode shows peaks related to both metallic bismuth and indium. Similar to the In-powder substrate, in the XRD pattern of the Bi–In-powder electrode recorded after 200 cycles, the reflections of both metallic bismuth and metallic indium did not show any significant shift, indicating that both bismuth and indium did not form an alloy with the zinc during the Zn deposition/dissolution cycles. The reflections related to the zinc hydroxy sulphate [Zn<sub>4</sub>(OH)<sub>6</sub>SO<sub>4</sub>·nH<sub>2</sub>O]<sup>[40]</sup> are visible within the diffractogram of the cycled Bi–In-powder electrode. However, contrary to the case of both the Bi-powder substrate (Figure SI\_3), a lower number of reflections related to the zinc hydroxy sulphate appeared within the diffractogram of the cycled Bi–In-electrode. This suggests that further Zn-based passivation products are formed with a lower appreciable amount onto the Bi–In-powder substrate, in accordance with the galvanostatic profile not showing any reductive spike at the beginning of the

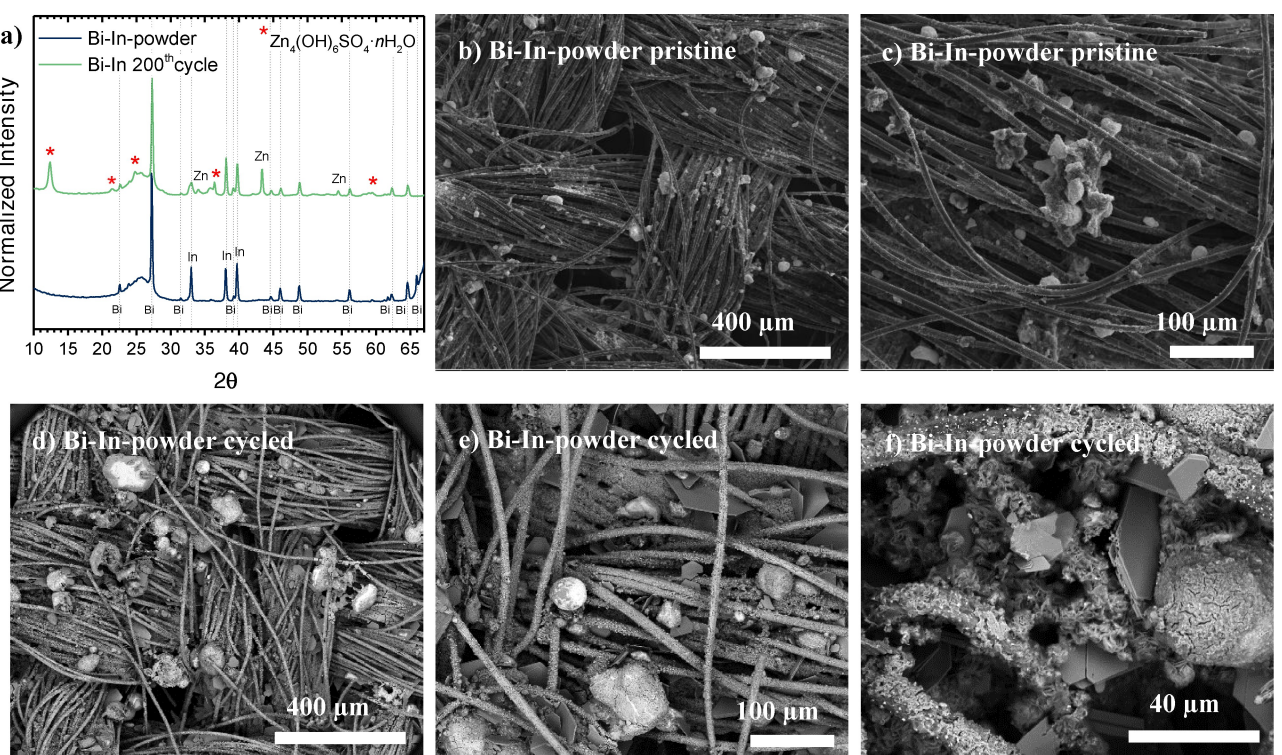


**Figure 4.** a) XRD pattern of a Bi–In-powder electrode before and after 200 zinc electro-deposition/dissolution cycles in 500 mM  $ZnSO_4$ . The reflections corresponding to zinc hydroxy sulphate  $Zn_4(OH)_6SO_4 \cdot nH_2O$  have been marked with (\*). SEM images of a Bi–In-powder electrode b, c) before and d–f) after 200 galvanostatic cycles recorded in 500 mM  $ZnSO_4$ . The current applied to the Bi–In-powder electrode was set in order to achieve a depth of discharge of 50%. All the SEM images of the cycled electrodes have been acquired after a Zn-stripping step.

Zn deposition step (Figure 3a).<sup>[25]</sup> According to the SEM images shown in Figure 4, the deposition of metallic zinc occurred very homogeneously onto the Bi–In-powder substrate without any appreciable formation of dendrites. The morphology of the pristine electrode was characterized by metallic particles distributed on top of the fibers of the carbon cloth current collector (Figure 4b and c). After 200 cycles, the electrode's morphology remained almost unaltered, with the carbon cloth's fibers clearly visible as shown in Figure 4(d–f). The zinc deposits looked homogeneously distributed onto the carbon fibers and the metallic particles (Figure 4f). Occasionally, few lamellar-shaped crystals most likely constituting the Zn-based double layered hydroxide species (such as the zinc hydroxy sulphate)<sup>[25,41]</sup> can be seen, however, their amount is extremely low compared to the case of the cycled Zn-powder electrode (Figure 2e and Figure f). The SEM images of the Bi–In powder electrode after the first Zn dissolution step are shown in Figure SI\_5 in the Supporting Information, section 5.

It is worth noticing that even if the zinc was deposited homogeneously onto the fibers of the carbon cloth current collector of the Bi–In-powder electrode (Figure 4d–f), such effect is to be ascribed to the presence of the indium within the electrode's formulation, and not to the carbon fibers themselves. In fact, the carbon itself generally behaves as an extremely poor substrate for the zinc deposition reaction, as demonstrated by the galvanostatic profile, the Coulombic efficiency and the morphology of a cycled carbon-powder electrode shown in the Supporting Information Sections 6 and

7 (the composition of the carbon-powder electrode can be found in Table 1).

To have a qualitative insight on how favored the hydrogen evolution is during the Zn electrodeposition step as a function of the substrate employed, the  $\Delta E_{\text{spike}}$  has been calculated as the difference between the mean value of the stationary Zn deposition potential ( $E_{\text{plateau}}$ ) and the initial reductive spike at the beginning of the reduction phase of the galvanostatic cycles ( $E_{\text{spike}}$ ), as suggested in previous work,<sup>[25]</sup> and visually depicted in Figure 5(a). This parameter  $\Delta E_{\text{spike}}$ , which can strongly affect the Zn electrodeposition efficiency,<sup>[25]</sup> has been calculated for the initial 60 dissolution/deposition cycles on all the different substrates employed in the frame of this work, as shown in Figure 5(b). It is worth noticing that during this set of experiments, the Bi-, Bi–In- and In-powder electrodes were not plated with 5 mg of zinc prior to the galvanostatic cycling employed for the estimation of the  $\Delta E_{\text{spike}}$ , to directly visualize the effect of the various substrates on the zinc deposition/dissolution reaction. The higher  $\Delta E_{\text{spike}}$ , the more negative is the initial cathodic potential spike compared to the stationary Zn deposition potential, and consequently, the higher the driving force for the evolution of gaseous  $H_2$ , according to the Butler-Volmer equation.<sup>[47]</sup> As shown in Figure 5(b), the Bi–In-powder electrode exhibited the lowest  $\Delta E_{\text{spike}}$  value, suggesting that this substrate is characterized by a higher overpotential towards the hydrogen evolution reaction, which leads to a better hindering of the formation of gaseous  $H_2$  during the Zn deposition step.

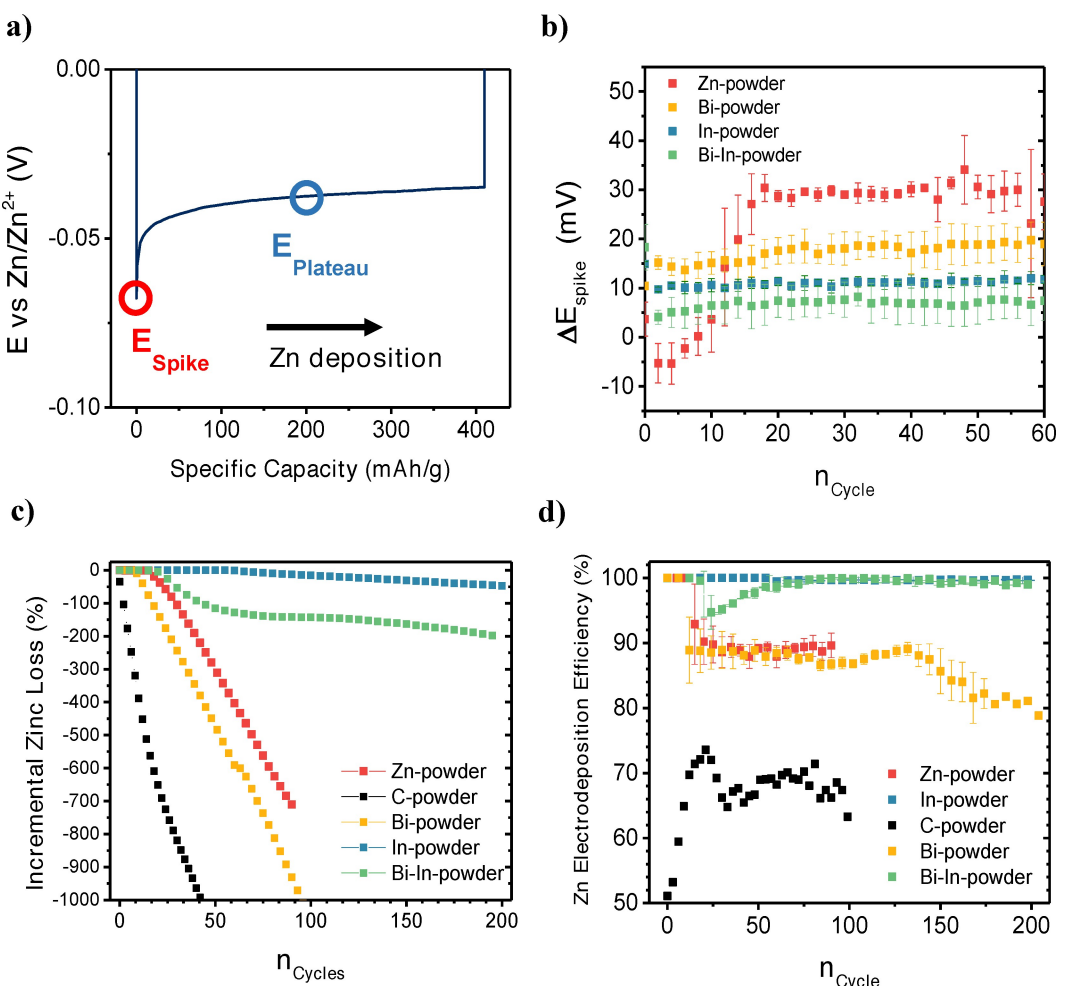


**Figure 5.** a) Representative reductive portion of a galvanostatic cycle during which the Zn electrodeposition step takes place; b) Average  $\Delta E_{\text{spike}}$  for different electrodes during galvanostatic cycling. c) Incremental loss of zinc mass for the different powder electrodes employed in the frame of this work cycled in a solution of 500 mM  $ZnSO_4$ ; d) average zinc electrodeposition efficiency of different powder electrodes cycled in 500 mM  $ZnSO_4$ . The mean values of the  $\Delta E_{\text{spike}}$  and of the Coulombic efficiency together with their relative standard deviations have been calculated from the results of three different measurements.

Subsequently, to assess the practical feasibility of the developed substrates for the Zn electrodeposition/dissolution reaction, the incremental loss of zinc mass per cycle has been estimated. This quantity, which is a direct consequence of the Zn electrodeposition efficiency, is a crucial parameter for the design of a practical Zn-ion battery, as it represents the cumulative amount of zinc that is lost compared to the amount of zinc that is deposited per cycle (details on the calculation of this quantity can be found within the Experimental Section).

In other words, the incremental zinc loss is an estimation of the amount of metallic zinc that has to be placed within an aqueous Zn-ion battery to act as a reservoir in order to ensure the battery operation for a specified number of cycles. Considering that usually the positive electrode's materials for aqueous Zn-ion batteries have a Coulombic efficiency close to 100%,<sup>[48]</sup> it is the Coulombic efficiency of the negative electrode the real bottleneck that dictates the amount of metallic zinc needed as a reservoir in the final aqueous Zn-ion cell. The calculated incremental Zn loss of all the electrodes used as the substrate for the Zn electrodeposition-dissolution reaction

within the frame of this work is shown in Figure 5(c). From this figure, it can be argued that when using a standard Zn-powder electrode, a metallic zinc reservoir of ca. 8 times higher than the capacity of the cathode (having a Coulombic efficiency of 100%) must be present within the electrode formulation to allow the Zn-ion battery to reach 100 cycles. When using an In-powder substrate, the amount of extra metallic zinc to be added within the electrode to act as a reservoir is ca. 0.5 times higher than the capacity of the cathode to let the Zn-ion cell run for 200 cycles. In the case of the more application feasible Bi-In-powder electrode, an extra zinc reservoir of ca. 2 times higher than the capacity of the cathode must be added to allow the Zn-ion cell to cycle for 200 cycles.

The striking differences in the amount of extra zinc needed as a reservoir as a function of the substrate used for the electrodeposition/dissolution reaction are the clear consequence of the Zn electrodeposition efficiency (Figure 5d). From a zinc reservoir point of view, it might sound appealing at first glance to work with Zn-powder negative electrodes, since they would provide an ideally unlimited zinc reservoir during the

Zn-ion battery operation. However, the massive amount of extra zinc that is present within the Zn ion cell, which is needed to counterbalance the poor Coulombic efficiency of the Zn-powder electrode itself, would dramatically decrease the gravimetric energy density of the final Zn-ion cell, which is expressed in  $\text{Wh kg}^{-1}$ . Therefore, substrates ensuring a Zn-electrodeposition efficiency as high as possible with the minimum amount of metallic zinc within their formulation should be preferred, paying attention at the same time to their price and their easiness of manufacturing to be feasibly appealing for a real-life application.

To test the potential applicability of the newly-formulated Bi–In-based substrates as negative electrodes in a full Zn-ion cell, a pouch-cell has been assembled employing a positive electrode based on commercial  $\text{MnO}_2$  and a Bi–In-powder negative electrode. The electrochemical performance of this full cell has been compared to a standard one constituted of the same positive electrode and a Zn-powder negative electrode.

Both full cells were cycled with a current rate of 0.5 C. The galvanostatic cycles of the full cells are shown in Figures SI\_8 and SI\_9 of the Supporting Information, respectively. As shown in Figure 6a, when a standard Zn-powder electrode was used as the negative electrode, the initial full cell capacity was  $57 \text{ mAh g}_{\text{MnO}_2}^{-1}$ . A maximum full cell capacity of  $77 \text{ mAh g}_{\text{MnO}_2}^{-1}$  was reached after 6 cycles. Such behavior is typical of the  $\text{MnO}_2$ , which undergoes an activation process during its initial cycling in aqueous Zn-containing electrolytes.<sup>[49,50]</sup> However, the capacity of the full cell dropped very quickly reaching a value of  $61 \text{ mAh g}_{\text{MnO}_2}^{-1}$  after only 30 cycles and  $32 \text{ mAh g}_{\text{MnO}_2}^{-1}$  after 50 cycles, corresponding to a full cell capacity retention at 0.5 C of 80% and 40%, respectively. On the other hand, when a Bi–In-powder electrode was used as the negative electrode in the full Zn-ion cell, the initial capacity of the full cell was  $70 \text{ mAh g}_{\text{MnO}_2}^{-1}$  and it increased reaching a maximum of  $104 \text{ mAh g}_{\text{MnO}_2}^{-1}$  around the 50th cycle, due to the activation of the  $\text{MnO}_2$ .<sup>[49,50]</sup> After the 50th cycle, the full cell capacity started decreasing and reached a value of  $81 \text{ mAh g}_{\text{MnO}_2}^{-1}$  after 300 cycles, corresponding to a full cell capacity retention at 0.5 C of 78%. Therefore, the use of the Bi–In-powder negative electrode prolonged the cycle life of the full Zn-ion cell 10 times. From the galvanostatic curves (see Figures SI\_8 and SI\_9), it can be noticed that while the Zn-powder-based full cell is clearly limited by the performance of the metallic zinc anode, the Bi–In-powder-based full cell is limited by the performance of the cathode. This means that a cycle life of the Bi–In-based full cell longer than the 300 cycles reached during this experiment can be potentially reached by using other cathode materials.

The Coulombic efficiency of both the full cells (Figure 6b) started with values higher than 100%, due to the initial activation process of the  $\text{MnO}_2$ -based positive electrode.<sup>[49,51]</sup> However, its evolution with the cycle number depended on the nature of the negative electrode. When a Zn-powder electrode was used, the efficiency quickly dropped from 100% to 96% after ca. 35 cycles. On the other hand, when a Bi–In-powder electrode was used as the negative electrode, the Coulombic

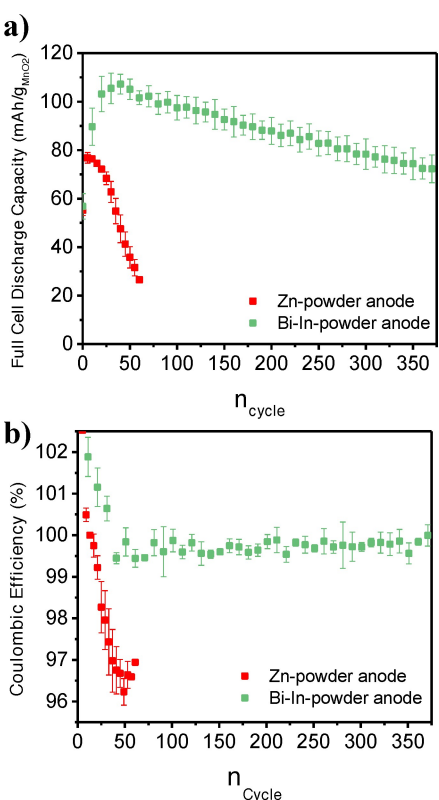


**Figure 6.** a) Average discharge capacity and b) Coulombic efficiency of two full pouch-cells assembled using two different negative electrodes (either Bi–In-powder or Zn-powder electrode). Both Zn-ion full cells were constituted of a  $\text{MnO}_2$ -based positive electrode, and a degassed 500 mM  $\text{ZnSO}_4$  aqueous electrolyte embedded within a glass fiber separator. The full cells were cycled with an applied current of  $1 \text{ mA cm}^{-2}$ , corresponding to a C-rate of 0.5 C. The mean values of the discharge capacity and of the Coulombic efficiency together with their relative standard deviations have been calculated from the results of three different measurements.

efficiency of the full cell remained at ca. 99.7% for 300 cycles, further demonstrating the applicability of such electrode in a full Zn-ion cell setup and its superiority compared to a standard Zn-powder negative electrode. Also in this case, the observations on such small fluctuations (of ca. 4%) of the Coulombic efficiency could be made thanks to the appropriate magnified scale and small marker employed in Figure 6b, which is in contrast to the ones routinely employed within the literature, spanning from 0% to 120% and using markers of ca. 5%, which make impossible to observe such small efficiency fluctuations.<sup>[52,53]</sup>

Finally, *operando* differential electrochemical mass spectrometry (DEMS) has been employed to quantitatively measure the hindering effect towards the hydrogen evolution reaction when electrodes containing metallic indium particles were used as substrates for the  $\text{Zn}^{2+}$  electrodeposition/dissolution reaction, in contrast with the standard Zn-powder electrode. The *operando* DEMS analysis has been performed on both the full cells assembled with a  $\text{MnO}_2$  cathode, and a Zn-powder or a Bi–In-powder anode, respectively. The amount of  $\text{H}_2$  evolved during the initial cycles of two different Zn-ion full cells

constituted of a Zn-powder, and of a Bi–In-powder negative electrode are shown in Figure 7(a) and (b), respectively.

In both the Zn-ion cells, gaseous hydrogen is evolved once the current starts flowing, with an amount that is dependent on the anode used. In particular, the use of Bi–In-powder anode reduced by three times the amount of nmol of evolved H<sub>2</sub>. As shown in Figure 7(a), the hydrogen evolution rate on a Zn-powder anode quickly reaches 10 nmol min<sup>-1</sup> in the first cycle and it remains above 10 nmol min<sup>-1</sup> for all the measurements, with evolution peaks during charge of the Zn-ion cell

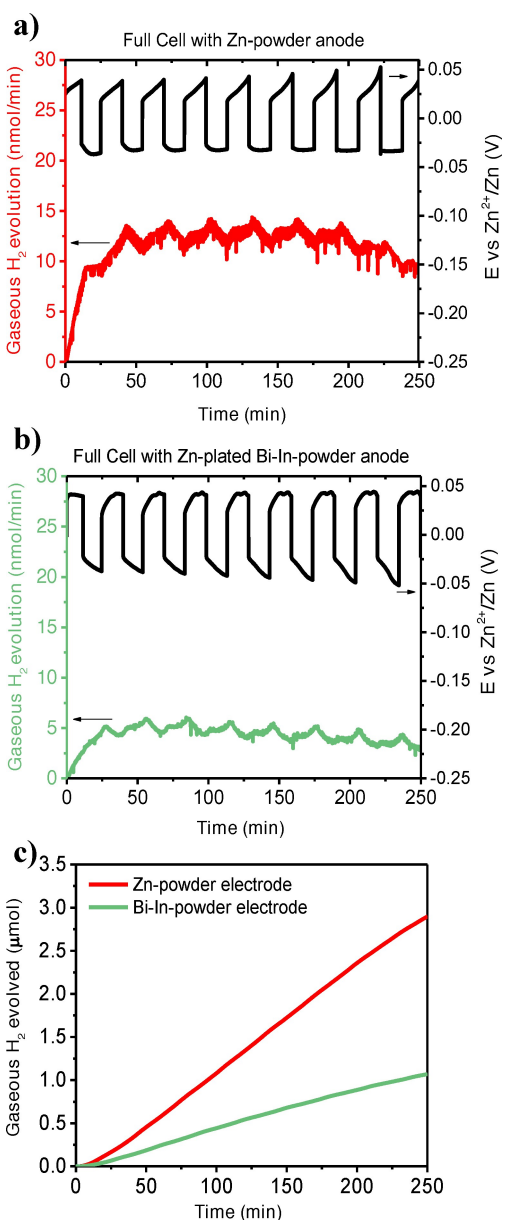


**Figure 7.** Quantitative evolution of gaseous hydrogen from a full Zn-ion cell using a) Zn-powder electrode or b) Bi–In electrode plated with 5 mg cm<sup>-2</sup> of zinc as the anode. c) Cumulative evolution of gaseous hydrogen evolved from a full Zn-ion cell constituted of a Zn-powder anode or a Bi–In electrode. Both Zn-ion full cells were constituted of a MnO<sub>2</sub>-based positive electrode and a degassed 500 mM ZnSO<sub>4</sub> aqueous electrolyte embedded within a glass fiber separator. The full cells were cycled with an applied current of 1 mA cm<sup>-2</sup>, corresponding to a C-rate of 0.5 C.

around 14 nmol min<sup>-1</sup>. In comparison, as shown in Figure 7(b), the hydrogen evolution rate on a Bi–In-powder electrode plated with 5 mg cm<sup>-2</sup> of zinc remains around 5 nmol min<sup>-1</sup> with evolution peaks around 6 nmol min<sup>-1</sup> despite being cycled with the same current density. It is worth noticing in Figure 7 that the hydrogen evolution follows a precise saw-like trend during the galvanostatic charge/discharge cycles. During the cell discharge (i.e., during the Zn dissolution step) the amount of H<sub>2</sub> evolved increases most likely because of the oxidative dissolution<sup>[54–56]</sup> of the native thin layer of insulating/poorly conductive Zn-based compounds (such as hydroxides, carbonates, etc.),<sup>[54–56]</sup> which always covers the surface of the metallic Zn particles when exposed to air and moisture.<sup>[54–56]</sup> Moreover, a peak in the amount of evolved hydrogen can be observed at the beginning of each cell charge (i.e., at the beginning of the Zn electrodeposition step). In this case, the surface of the metallic zinc is now exposed to the solution, as the native thin layer of Zn-oxides/carbonates has been oxidized during the discharge, the reduction of water resulting in the evolution of gaseous hydrogen is enhanced by the negative polarization of the electrode. After this initial phase of the zinc electrodeposition step, the surface of the electrode is slowly covered again with zinc oxides/hydroxides-based compounds due to the local pH increase that is caused by the hydrogen evolution. The presence of these compounds on the surface of the electrode, in turn, causes a slow decrease in the H<sub>2</sub> evolution rate as well.

Interestingly, by observing the overall signal of the evolved hydrogen over the whole time-span represented in Figure 7, it can be noticed that the overall rate of H<sub>2</sub> evolved slowly decreases during the cycles, going from a maximum of ca. 14 to 10 nmol min<sup>-1</sup> on a Zn-powder anode (Figure 7a) and from a maximum of ca. 6 to 2.5 nmol min<sup>-1</sup> on a Bi–In-powder anode (Figure 7b). Such overall slow decrease of the amount of gaseous H<sub>2</sub> evolved during the cycles is symptomatic of the formation and accumulation of zinc oxide-/hydroxide-based passivation products on the surface of the electrodes,<sup>[13,38]</sup> occurring in a higher extent in the case of the conventional Zn-powder anode. This is in total agreement with the SEM postmortem analysis, which showed a strong change in the morphology of the cycled Zn-powder electrode with a strong build-up of lamellar shaped compounds (Figure 2e and f), and on the other hand a morphology of the cycled Bi–In-powder electrode very similar to the pristine one, with the formation of only a few lamellar shaped particles.

The cumulative amount of gaseous hydrogen evolved during the initial cycles of the Zn-ion cells has been obtained integrating the gaseous H<sub>2</sub> evolution rate for both Zn-ion cells, as shown in Figure 7(c). After 250 min (ca. 4 h) of cycling, a total amount of 2.90 and 1.00 μmol of hydrogen have been evolving from the Zn-powder and the Bi–In-powder electrode, respectively. This is equal to a decrease of more than 65 % in terms of total amount of evolved hydrogen when employing the Bi–In-powder substrate, with respect to the conventional Zn-powder one.

Due to the excellent performance of the Bi–In-powder substrate as a potential negative electrode for aqueous Zn-ion

cells, and to its hindering effect towards the gaseous H<sub>2</sub> evolution reaction proved by the *operando* DEMS analysis (Figure 7), it is worth making some economic considerations in order to assess the feasibility of its application. The cost of metallic bismuth (5.7 \$ kg<sup>-1</sup>) is close to the one of metallic Zn (3.5 \$ kg<sup>-1</sup>), while the cost of metallic indium (180 \$ kg<sup>-1</sup>) is ca. 50 times higher.<sup>[45,46]</sup> Therefore, at first glance, the use of 10 wt % of metallic indium within the Bi–In-powder electrode formulation would make this at least 5 times more expensive than a standard Zn-powder one. However, the use of 10 wt% of indium particles within the Bi–In-powder electrode leads to at least 10 times longer cycle life of the full cell. Therefore, the use of a standard Zn-powder electrode would imply a mass loading of metallic zinc of one order of magnitude higher than the one required by the Bi–In-powder electrode to allow the Zn-ion battery to cycle as long as the Bi–In-based one. This would make the cost of the Bi–In-powder electrode comparable if not even lower than the one of a standard Zn-powder electrode.

Lastly, in order to further stress the excellent performance of the proposed Bi–In-powder electrode, important performance quantifiers for the Zn electrodeposition/dissolution reaction in aqueous Zn-ion batteries (such as: Coulombic efficiency, specific capacity, depth of discharge, amount of metallic zinc electrodeposited/dissolved during the cycles, applied current, etc.) have been extensively compared with the values already reported in the literature, as shown in Table SI\_1 within the Supporting Information, Section 10. All the values obtained from the literature for the comparison, are referred to half-cell tests. The average Coulombic efficiency of the Bi–In-powder electrode of 99.4% (Figure 5) is the highest among the ones clearly reported within the literature. To the best of our knowledge, a slightly higher average Coulombic efficiency value of 99.5% has been reached using a Pt electrode in a high concentrated electrolyte containing 20 M LiTFSi.<sup>[32]</sup> However, platinum substrates are not appealing at all for a realistic application in aqueous Zn-ion batteries due to their high costs, and the current density employed in the work of Wang et al.<sup>[32]</sup> was 0.2 mA cm<sup>-2</sup>, ten times lower than the more realistic one employed in this study (2 mA cm<sup>-2</sup>).

Metallic indium has been deposited onto a zinc foil by Han et al.<sup>[52]</sup> and Hu et al.<sup>[57]</sup> However, not only these studies do not show in an appropriately clear way the Coulombic efficiency values obtained with the In-plated substrates, but also, in one case,<sup>[52]</sup> the amount of zinc electrodeposited/dissolved during the cycles (i.e., depth of discharge) was not given and, in another case,<sup>[57]</sup> it was only 1.5% of the weight of the In-plated Zn anode, in contrast to the more realistic depth of discharge value (of 50%) employed in this work. In the study of Hu et al.<sup>[57]</sup> it was even claimed by the authors that the In layer would act as solid electrolyte interphase (SEI), despite metallic indium is an electronic conductor, in contrast to the solid electrolyte interphase which, by definition, is an electronic insulator and an ion conductor.<sup>[58–61]</sup> Moreover, in both studies the amount of metallic indium employed within the electrode formulation was ca. 3.5<sup>[52]</sup> and 7 mg cm<sup>-2</sup>.<sup>[57]</sup> These values, being three and seven times more than the metallic indium employed

within the Bi–In-powder formulation proposed within this work, would result in higher electrode costs.

## Conclusion

Despite the research efforts that have been focused on aqueous ZIBs in recent years, the poor Zn electrodeposition efficiency in mild-acidic electrolytes remains the bottleneck that hinders the commercialization of neutral aqueous Zn-ion batteries. Such low Coulombic efficiency is mainly due to the unwanted formation of gaseous H<sub>2</sub> occurring concomitantly to the Zn deposition step. The parasitic hydrogen evolution reaction leads to a variety of detrimental effects on the operation of an overall Zn-ion battery, such as (I) pressure build-ups within the Zn-ion cell, (II) decrease of the portion of electric current that is actually employed for the deposition of metallic zinc and (III) loss of active Zn<sup>2+</sup> due to the local increase of pH in the proximity of the negative electrode, which promotes the formation and the stabilization of unwanted Zn oxide/hydroxide-based species. Despite the clear negative effects of the parasitic hydrogen evolution reaction, little work has been focused on effectively tackling this issue.

Here, the Zn electrodeposition efficiency has been increased by using an electrode containing metallic Indium as a substrate for the Zn electrodeposition and dissolution reaction. Indium (In) is a non-toxic, environmentally friendly metal, which exhibits very poor hydrogen evolution kinetics. The Zn deposition/dissolution reaction onto a substrate constituted mainly of metallic In particles was characterized by a stable Coulombic efficiency of ca. 99.8% for 200 subsequent cycles, and by very homogeneous and dendrite-free Zn deposits. Considering the high market price of Indium, a Bi–In-based electrode containing only 10 wt% of metallic indium particles has been prepared to reduce the amount of metallic indium within the electrode formulation, while keeping at the same time a high zinc electrodeposition efficiency at realistic current and charge densities (2 mA cm<sup>-2</sup> and 2 mAh cm<sup>-2</sup>). The Bi–In-based electrode appeared to be effective in hindering the hydrogen evolution reaction during the Zn dissolution/deposition. In fact, it allowed a Zn electrodeposition efficiency of ca. 99.4% for 200 subsequent galvanostatic cycles. The morphological analysis demonstrated that this formulation led to dendrite-free, highly homogeneous Zn deposits all over the electrode surface, contrary to the conventional Zn-based paste electrodes. Moreover, the use of Bi–In electrodes allowed a strongly reduced incremental Zn loss compared to the standard Zn-based electrodes (namely 150% and 800%, respectively after 100 cycles). Consequently, the use of Bi–In electrode requires a much smaller Zn mass reservoir to ensure the correct operation of the final Zn-ion battery, even in the case of higher depths of discharge for the zinc-based electrode. The direct comparison in full zinc-ion cells of the Bi–In and Zn-based anodes has underlined further the advantage of the former over the latter: not only the cycle life of the full pouch cell was enhanced by 10 times, but also the anode was no longer the limiting component of the cell. This indicates a clear advantage

not only in terms of the gravimetric energy density of the final Zn-ion cell, but also makes the Bi–In-powder electrodes economically competitive. Quantitative *operando* differential mass spectrometry (DEMS) coupled with galvanostatic cycling has revealed that gaseous hydrogen is always evolving with variable intensity on the negative electrode's surface (i.e., during both the charge and the discharge of the Zn-ion cell), whose amount is dependent on the substrate employed for the zinc electrodeposition/dissolution reaction, even when substrates containing indium have been used. This crucial result suggests that the parasitic H<sub>2</sub> evolution reaction although it can be strongly reduced, it can never be completely suppressed in aqueous electrolytes on Zn-based electrodes. Therefore, a quantitative evaluation of the gas evolved from full ZIBs should always be included in every study about the zinc electrodeposition efficiency. This side reaction can be at most hindered from a kinetic point of view and, according to the aforementioned requirements for competitive and realistic aqueous zinc batteries, this should always be done through the employment of safe, cheap and recyclable solutions and materials.

Considering the non-toxicity, environmental friendliness and easiness of the electrode manufacturing process, Bi–In powder electrodes, in comparison to the state-of-the-art substrates already reported in the literature, are extremely promising as a feasible route to achieve dendrite-free and high zinc electrodeposition efficiencies (99.4%) in mild aqueous Zn-ion batteries, for prolonged cycling.

## Experimental Section

### Electrode preparation

Metallic particles of zinc (purum, Sigma Aldrich), indium (99.99%, 100 mesh, Sigma Aldrich) and bismuth (99.5%, 100 mesh, Alfa Aesar) have been used as purchased for the electrodes' preparation. All the metallic particles-based electrodes have been prepared by brush-coating carbon cloth strips (Carbon Fabric 1071, AvCarb) with a liquid slurry consisting of metallic powder, conductive carbon additive (Super C65, Timcal) and polyvinylidene fluoride (PVDF, Solef S5130, Solvay) dissolved in N-methyl-2-pyrrolidone (NMP, Sigma Aldrich), using the weight ratios reported in Table 1. The mixture was stirred for a total of 30 min at 4000 rpm using a turbo-mixer (Ultra-Turrax, IKA) and brushed to get an apparent coated surface of ca. 1 cm<sup>2</sup>. The coated carbon strips were then dried overnight at 60°C. The average mass loading of the metallic powders on the electrodes was ca. 10 mg cm<sup>-2</sup>. All the electrodes have been washed for 90 sec in 1 M hydrochloric acid just before being inserted into the electrochemical cell, prior to any test, in order to remove any oxide layer present on the metallic particles' surface.

### Stripping/plating tests

All the stripping-plating tests have been carried out in three-electrode electrochemical cells, using two zinc foils ( $\geq 99.9\%$ , Goodfellow) as the reference and counter electrode, respectively. An aqueous solution of 500 mM ZnSO<sub>4</sub> (monohydrate,  $\geq 99.9\%$ , Sigma Aldrich) has been used as the electrolyte. To reduce the oxygen content in the electrolyte, the solution was degassed by

sonication under vacuum for 30 min and bubbled with pure argon for 1 h prior to any measurement. To avoid oxygen's presence during the measurements, every electrochemical cell was fluxed with argon for 15 min during its assembly and kept under argon during the entire duration of the electrochemical measurements. All the electrochemical tests have been carried out with the aid of a Biologic VMP3® potentiostat. The zinc electrodeposition efficiency was calculated from the galvanostatic cycling with potential limitation (GCPL) as the ratio between the electric charge retrieved in the stripping step (oxidation) and the one involved in the plating step (reduction). For each measurement, the upper potential limit has been set at 200 mV versus the redox potential of zinc, while the maximum plating time has been set to 1 h. The applied current was calculated in such a way to strip and plate half of the total mass of zinc on each electrode (thus applying a depth of discharge of 50% to the anode of each cell). Since the Bi-powder, In-powder and Bi–In-powder electrodes did not contain any amount of Zn within their initial formulation, these electrodes have been plated with 5 mg cm<sup>-2</sup> of metallic zinc (corresponding to 4.1 mAh cm<sup>-2</sup>) prior to any measurement. Every galvanostatic measurement was set to start with a Zn deposition sequence.

The incremental loss of zinc from the working electrode was calculated according to the following equation:

$$\%m_{Zn,n} = \sum_1^n \left( 1 - \frac{Q_{an,n}}{Q_{cat,n}} \right) \cdot 100$$

where  $\%m_{Zn,n}$  is the incremental loss of zinc at the  $n^{th}$  cycle,  $Q_{an,n}$  is the anodic charge retrieved in the stripping step (oxidation) at the  $n^{th}$  cycle, and  $Q_{cat,n}$  is the cathodic charge involved in the plating step (reduction) at the  $n^{th}$  cycle.

### Zn-ion full-cell assembly and electrochemical tests

Full Zn-ion cells (pouch-cells) have been assembled using a degassed ZnSO<sub>4</sub> 500 mM aqueous solution as the electrolyte, a positive electrode constituted of manganese(IV) dioxide (MnO<sub>2</sub> 99.99% Sigma Aldrich) as active material, and Bi–In negative electrode plated with zinc or a Zn-powder negative electrode, respectively. The formulations of the Bi–In-powder electrode and of the Zn-powder electrode are reported in Table 1. The manganese oxide-based positive electrode has been prepared following the same procedure described above with the constituents MnO<sub>2</sub> : C65 : PVDF having the following weight ratios 80:10:10 wt%. All the slurries of both the positive and the negative electrodes have been brush-coated onto L-shaped carbon cloth current collectors having an apparent surface of 4 cm<sup>2</sup>. The mass loading for both the positive and negative electrodes was ca. 7 mg cm<sup>-2</sup>. Prior to the assembly of the pouch cells, the negative electrode (Bi–In-powder or Zn-powder) has been washed with 1 M HCl for 90 sec and successively rinsed with deionized water. After the washing step, ca. 5 mg cm<sup>-2</sup> (thus 4.1 mAh cm<sup>-2</sup>) of metallic Zn have been electrodeposited onto the surface of the Bi–In-powder electrode, which was immersed within a beaker containing a solution of 500 mM ZnSO<sub>4</sub>, and two L-shaped zinc plates ( $\geq 99.9\%$ , Goodfellow) acting as counter and reference electrodes, respectively. A current density of 2.05 mA cm<sup>-2</sup> was applied for 2 h in order to deposit the amount of metallic zinc. Pouch cells with a dimension of 7 cm  $\times$  7 cm have been assembled using two layers of glass microfiber papers (Whatman) with a dimension of 3 cm  $\times$  3 cm to act as separators. The glass separator was then wetted with 700  $\mu$ L of electrolyte. The electrodes and the wetted separator have then been sealed under vacuum using a total pressure of 200 mbar. The final pouch cells have been pressed between two aluminium plates after their assembly to ensure the stability of the electric contacts.

All the pouch cells have been electrochemically tested with the aid of a Biologic VMP3® potentiostat with a current rate of 0.5 C.

### Materials characterization

The morphology, the phase composition and the crystallinity of every electrode were analyzed with the aid of X-ray powder diffraction (XRPD) and scanning electron microscopy (SEM) coupled with energy-dispersive X-ray spectroscopy (EDS).

SEM images were acquired at different magnifications using an FEI Helios NanoLan 600 DualBeam® apparatus with an acceleration voltage of 10 kV, a beam current of 0.14 nA. Every sample was analyzed without using any conductive coating, due to the high electric conductivity of the electrodes themselves.

The XRPD diffractograms were obtained between 10° and 65° in the 2θ range using a Miniflex Rigaku® instrument for powder analyses. The signal was acquired every 0.03° with a scan speed of 5 seconds/step. For this analysis, every electrode was ground in an agate mortar and then homogeneously deposited on a silicon plate using isopropanol. The silicon plate was then dried and secured to the instrument's sample holder using two tape strips. Every diffractogram was normalized using the intensity of the carbon peak identified at 25.7°.

### Operando DEMS analysis

A poly ether ketone (PEEK) electrochemical cell for differential electrochemical mass spectrometry (DEMS) analysis designed *in-house* has been used to perform the *operando* analysis of the gas evolved during the galvanostatic cycling of the Zn-ion battery.<sup>[62]</sup> DEMS cells were assembled using 200 μL of de-aerated 500 mM ZnSO<sub>4</sub> solution as the electrolyte, a zinc plate as reference electrode, a positive electrode consisting of manganese(IV) dioxide as active material and a negative electrode consisting either of Zn-powder or Bi-In-powder. Prior to the DEMS experiments, the Bi-In electrode was washed 5 mg cm<sup>-2</sup> of zinc were previously plated following the procedures described previously. Every cell was tested with the aid of a Biologic VMP3® potentiostat with a current rate of 0.5 C in order to replicate the experimental conditions used with the full Zn-ion pouch cells. Moreover, 0.2 sccm min<sup>-1</sup> of argon (Ar 5.0) were flown into the cell during all the tests, with the aid of a mass flow controller (Alicat Scientific). An auxiliary argon flow of 1 sccm min<sup>-1</sup> was run in parallel to the main cell flow in order to have a total gas output of 1.2 sccm to the mass spectrometer. The evolution of gaseous hydrogen from the Zn-ion full cells was quantified using a quadrupole mass spectrometer (Thermostar™, Pfeiffer Vacuum) which had been carefully calibrated for quantifying the I<sub>2</sub> signal according to previous work.<sup>[63]</sup> The internal pressure of the instrument was set to 7 × 10<sup>-7</sup> mbar during every experiment.

### Acknowledgements

The financial support of the Federal Ministry of Education and Research (BMBF) in the framework of the project "ZIB" (FKZ 03XP0204A) is gratefully acknowledged. Open Access funding enabled and organized by Projekt DEAL.

### Conflict of Interest

The authors declare no conflict of interest.

### Data Availability Statement

The data that support the findings of this study are available from the corresponding author upon reasonable request.

**Keywords:** aqueous zinc-ion batteries • bismuth • cycle life • dendrites • full Zn-ion cell • indium • metallic zinc anode • parasitic hydrogen evolution

- [1] V. Verma, S. Kumar, W. Manalastas, R. Satish, M. Srinivasan, *Adv. Sustainable Syst.* **2019**, *3*, 1800111.
- [2] V. Blay, R. E. Galian, L. M. Muresan, D. Pankratov, P. Pinyou, G. Zampardi, *Adv. Sustainable Syst.* **2020**, *4*, 1–14.
- [3] G. Fang, J. Zhou, A. Pan, S. Liang, *ACS Energy Lett.* **2018**, *3*, 2480–2501.
- [4] G. Zampardi, F. La Mantia, *Curr. Opin. Electrochem.* **2020**, *21*, 84–92.
- [5] H. Ao, Y. Zhao, J. Zhou, W. Cai, X. Zhang, Y. Zhu, Y. Qian, *J. Mater. Chem. A* **2019**, *7*, 18708–18734.
- [6] J. Shin, J. Lee, Y. Park, J. W. Choi, *Chem. Sci.* **2020**, *11*, 2028–2044.
- [7] B. Tang, L. Shan, S. Liang, J. Zhou, *Energy Environ. Sci.* **2019**, *12*, 3288–3304.
- [8] A. Konarov, N. Voronina, J. H. Jo, Z. Bakenov, Y. K. Sun, S. T. Myung, *ACS Energy Lett.* **2018**, *3*, 2620–2640.
- [9] G. Kasiri, J. Glenneberg, A. Bani Hashemi, R. Kun, F. La Mantia, *Energy Storage Mater.* **2019**, *19*, 360–369.
- [10] G. Kasiri, J. Glenneberg, R. Kun, G. Zampardi, F. La Mantia, *ChemElectroChem* **2020**, *7*, 3301–3310.
- [11] T. Yamamoto, T. Shoji, *Inorg. Chim. Acta* **1986**, *117*, 27–28.
- [12] P. Yu, Y. Zeng, H. Zhang, M. Yu, Y. Tong, X. Lu, *Small* **2019**, *15*, 1–27.
- [13] F. Argoul, A. Kuhn, *J. Electroanal. Chem.* **1993**, *359*, 81–96.
- [14] G. Zampardi, R. G. Compton, *J. Solid State Electrochem.* **2020**, *24*, 2695–2702.
- [15] J. Hao, X. Li, S. Zhang, F. Yang, X. Zeng, S. Zhang, G. Bo, C. Wang, Z. Guo, *Adv. Funct. Mater.* **2020**, *30*, 1–10.
- [16] J. Hao, B. Li, X. Li, X. Zeng, S. Zhang, F. Yang, S. Liu, D. Li, C. Wu, Z. Guo, *Adv. Mater.* **2020**, *32*, 1–9.
- [17] Q. Zhang, J. Luan, L. Fu, S. Wu, Y. Tang, X. Ji, H. Wang, *Angew. Chem. Int. Ed.* **2019**, *58*, 15841–15847; *Angew. Chem.* **2019**, *131*, 15988–15994.
- [18] H. Li, C. Xu, C. Han, Y. Chen, C. Wei, B. Li, F. Kang, *J. Electrochem. Soc.* **2015**, *162*, A1439–A1444.
- [19] X. Shi, G. Xu, S. Liang, C. Li, S. Guo, X. Xie, X. Ma, J. Zhou, *ACS Sustainable Chem. Eng.* **2019**, *7*, 17737–17746.
- [20] T. Gupta, A. Kim, S. Phadke, S. Biswas, T. Luong, B. J. Hertzberg, M. Chamoun, K. Evans-Lutterodt, D. A. Steingart, *J. Power Sources* **2016**, *305*, 22–29.
- [21] M. Cui, Y. Xiao, L. Kang, W. Du, Y. Gao, X. Sun, Y. Zhou, X. Li, H. Li, F. Jiang, C. Zhi, *ACS Appl. Energ. Mater.* **2019**, *2*, 6490–6496.
- [22] L. Kang, M. Cui, F. Jiang, Y. Gao, H. Luo, J. Liu, W. Liang, C. Zhi, *Adv. Energy Mater.* **2018**, *8*, 1–8.
- [23] K. Zhao, C. Wang, Y. Yu, M. Yan, Q. Wei, P. He, Y. Dong, Z. Zhang, X. Wang, L. Mai, *Adv. Mater. Interfaces* **2018**, *5*, 1–7.
- [24] C. Shen, X. Li, N. Li, K. Xie, J. G. Wang, X. Liu, B. Wei, *ACS Appl. Mater. Interfaces* **2018**, *10*, 25446–25453.
- [25] A. Bani Hashemi, G. Kasiri, J. Glenneberg, F. Langer, R. Kun, F. La Mantia, *ChemElectroChem* **2018**, *5*, 2073–2079.
- [26] A. Naveed, H. Yang, J. Yang, Y. Nuli, J. Wang, *Angew. Chem. Int. Ed.* **2019**, *58*, 2760–2764; *Angew. Chem.* **2019**, *131*, 2786–2790.
- [27] Y. Cheng, L. Luo, L. Zhong, J. Chen, B. Li, W. Wang, S. X. Mao, C. Wang, V. L. Sprenkle, G. Li, J. Liu, *ACS Appl. Mater. Interfaces* **2016**, *8*, 2–9.
- [28] Z. Wang, J. Huang, Z. Guo, X. Dong, Y. Liu, Y. Wang, Y. Xia, *Joule* **2019**, *3*, 1289–1300.
- [29] K. E. K. Sun, T. K. A. Hoang, T. N. L. Doan, Y. Yu, X. Zhu, Y. Tian, P. Chen, *ACS Appl. Mater. Interfaces* **2017**, *9*, 9681–9687.
- [30] A. Bani Hashemi, G. Kasiri, F. La Mantia, *Electrochim. Acta* **2017**, *258*, 703–708.

- [31] Z. Liu, G. Pulletikurthi, F. Endres, *ACS Appl. Mater. Interfaces* **2016**, *8*, 12158–12164.
- [32] F. Wang, O. Borodin, T. Gao, X. Fan, W. Sun, F. Han, A. Faraone, J. A. Dura, K. Xu, C. Wang, *Nat. Mater.* **2018**, *17*, 543–549.
- [33] Z. Zhao, J. Zhao, Z. Hu, J. Li, J. Li, Y. Zhang, C. Wang, G. Cui, *Energy Environ. Sci.* **2019**, *12*, 1938–1949.
- [34] D. Yuan, W. Manalastas, L. Zhang, J. J. Chan, S. Meng, Y. Chen, M. Srinivasan, *ChemSusChem* **2019**, *12*, 4889–4900.
- [35] Q. Yang, G. Liang, Y. Guo, Z. Liu, B. Yan, D. Wang, Z. Huang, X. Li, J. Fan, C. Zhi, *Adv. Mater.* **2019**, *31*, 1903778.
- [36] G. Kasiri, R. Trócoli, A. Bani Hashemi, F. La Mantia, *Electrochim. Acta* **2016**, *222*, 74–83.
- [37] Y. Li, B. Liu, J. Ding, X. Han, Y. Deng, T. Wu, K. Amine, W. Hu, C. Zhong, J. Lu, *Batteries & Supercaps* **2021**, *4*, 60–71.
- [38] A. Bani Hashemi, F. La Mantia, *Anal. Chem.* **2016**, *88*, 7916–7920.
- [39] S. Trasatti, *J. Electroanal. Chem.* **1972**, *39*, 163–184.
- [40] A. Mozezzi, M. B. Cortie, A. M. McDonagh, *Dalton Trans.* **2013**, *42*, 14432–14437.
- [41] M. A. González, R. Trócoli, I. Pavlovic, C. Barriga, F. La Mantia, *Electrochim. Commun.* **2016**, *68*, 1–4.
- [42] P. Oberholzer, E. Tervoort, A. Bouzid, A. Pasquarello, D. Kundu, *ACS Appl. Mater. Interfaces* **2019**, *11*, 674–682.
- [43] Z. Li, S. Ganapathy, Y. Xu, Z. Zhou, M. Sarilar, M. Wagemaker, *Adv. Energy Mater.* **2019**, *9*, 1–10.
- [44] M. Pourbaix, *Atlas of Electrochemical Equilibria in Aqueous Solutions*, National Association of Corrosion Engineers, Houston, 1974.
- [45] Institut für seltene Erden und strategische Metalle, “Prices for strategic metals in December 2020,” can be found under <https://en.institut-seltene-erden.de/our-service-2/Metal-prices/strategic-metals-prices/>, 2020.
- [46] Institut für seltene Erden und strategische Metalle, “Base metals prices in December 2020,” can be found under <https://en.institut-seltene-erden.de/our-service-2/Metal-prices/Base-metals-prices/>, 2020.
- [47] A. J. Bard, L. R. Faulkner, *Electrochemical Methods Fundamentals and Applications*, 2<sup>nd</sup> edition, Wiley, New York, 2000.
- [48] G. Zampardi, M. Warnecke, M. Tribbia, J. Glenneberg, C. Santos, F. La Mantia, *Electrochim. Commun.* **2021**, *126*, 107030.
- [49] M. H. Alfaruqi, J. Gim, S. Kim, J. Song, D. T. Pham, J. Jo, Z. Xiu, V. Mathew, J. Kim, *Electrochim. Commun.* **2015**, *60*, 121–125.
- [50] G. G. Yadav, X. Wei, J. Huang, J. W. Gallaway, D. E. Turney, M. Nyce, J. Secor, S. Banerjee, *J. Mater. Chem. A* **2017**, *5*, 15845–15854.
- [51] G. G. Yadav, J. W. Gallaway, D. E. Turney, M. Nyce, J. Huang, X. Wei, S. Banerjee, *Nat. Commun.* **2017**, *8*, 1–9.
- [52] D. Han, S. Wu, S. Zhang, Y. Deng, C. Cui, L. Zhang, Y. Long, H. Li, Y. Tao, Z. Weng, Q. H. Yang, F. Kang, *Small* **2020**, *16*, 1–7.
- [53] Q. Jian, Z. Guo, L. Zhang, M. Wu, T. Zhao, *Chem. Eng. J.* **2021**, *425*, 130643.
- [54] S. Fajardo, G. S. Frankel, *Electrochim. Commun.* **2017**, *84*, 36–39.
- [55] A. Farooq, M. Hamza, Q. Ahmed, K. M. Deen, *Electrochim. Acta* **2019**, *314*, 135–141.
- [56] M. Curioni, L. Salamone, F. Scenini, M. Santamaría, M. Di Natale, *Electrochim. Acta* **2018**, *274*, 343–352.
- [57] K. Hu, X. Guan, R. Lv, G. Li, Z. Hu, L. Ren, A. Wang, X. Liu, J. Luo, *Chem. Eng. J.* **2020**, *396*, 125363.
- [58] G. Zampardi, R. Trocoli, W. Schuhmann, F. La Mantia, *Phys. Chem. Chem. Phys.* **2017**, *19*, 28381–28387.
- [59] G. Zampardi, F. La Mantia, *Batteries & Supercaps* **2020**, *3*, 672–697.
- [60] G. Zampardi, F. La Mantia, W. Schuhmann, *RSC Adv.* **2015**, *5*, 31166–31171.
- [61] G. Zampardi, F. La Mantia, W. Schuhmann, *Electrochim. Commun.* **2015**, *58*, 1–5.
- [62] A. Bani Hashemi, *Electrochemical and Morphological Characterization of the Interface At Negative Electrodes in Aqueous Metal-Ion Batteries*, PhD thesis, Universität Bremen (DE), 2018.
- [63] F. La Mantia, F. Rosciano, N. Tran, P. Novák, *J. Electrochem. Soc.* **2009**, *156*, A823.

Manuscript received: December 7, 2021

Revised manuscript received: December 21, 2021

Accepted manuscript online: January 18, 2022

Version of record online: February 3, 2022